

Dynamically stable topological edge states in an extended Su-Schrieffer-Heeger ladder with balanced perturbation

E. S. Ma,¹ K. L. Zhang,^{2,*} and Z. Song^{1,†}

¹*School of Physics, Nankai University, Tianjin 300071, China*

²*School of Physics and Optoelectronic Engineering, Foshan University, Foshan 528225, China*

The on-site potentials may break the symmetry of a system, resulting in the loss of its original topology protected by the symmetry. In this work, we study the counteracting effect of non-Hermitian terms on real potentials, resulting in dynamically stable topological edge states. We show exactly for a class of systems that the spectrum remains unchanged in the presence of balanced perturbations. As a demonstration, we investigate an extended non-Hermitian Su-Schrieffer-Heeger (SSH) ladder. We find that the bulk-boundary correspondence still holds, and the zero-energy edge states become coalescing states. In comparison to the original SSH chain, such edge states are robust not only against local perturbations but also in the time domain. As a result, a trivial initial state can always evolve to a stable edge state. Our results provide insights for the application of time-domain stable topological quantum devices.

I. INTRODUCTION

Topological phases are characterized by the global properties of a system, with one of their central ingredients being the topological edge states protected by topology and symmetry of the system [1–17]. Due to their resilience against local perturbations, topological edge states hold significant potential for quantum computing and highly robust devices [4, 6, 10, 18]. Nowadays, non-equilibrium topological phases and the dynamic manipulation of topological edge states have attracted great interest [19–29] due to the development of related experimental techniques in platforms such as ultracold atoms and optics. These advancements have enabled unprecedented control over quantum systems, allowing researchers to realize Floquet topological phases [19, 23] and topological charge pumping [20, 27] through different driving protocols. Notably, these platforms also allow us to introduce controllable gain and loss to achieve non-Hermitian topological Hamiltonians.

Non-Hermiticity not only expands the scope of topological phases research but also provides novel concepts and technical support for practical applications in fields such as optics and acoustics [30–43]. On the one hand, the asymmetric hoppings and gain-loss mechanisms in non-Hermitian systems offer additional degrees of freedom for regulating topological properties, enabling the existence of exotic edge states. Also, as the non-Hermitian skin effect (NHSE) may breaks the bulk-boundary correspondence (BBC) and the original topological edge states, new topological invariants are constructed to capture the topological properties of such systems [35–37]. On the other hand, non-Hermitian dynamics, such as exceptional point (EP) dynamics [44–48] and self-healing of non-Hermitian skin modes [49–51], provide a unique pathway for flexibly preparing and con-

trolling topological edge states through external parameters. Recent studies have revealed that topological skin-edge modes enabled by intrinsic non-Hermitian point-gap topology exhibit a remarkable self-healing wave feature, demonstrating unprecedented robustness against structural perturbations [49]. Based on these considerations, an intriguing question is that in the case of line-gap topology without NHSE, whether the non-Hermitian system support dynamically stable topological edge states with self-healing characteristic?

In this work, we consider this question by constructing a class of lattice model $\mathcal{H} = H_0 + H_p$, with Hermitian bipartite lattice H_0 and non-Hermitian perturbation term H_p consisting of real on-site potentials and imaginary hoppings. The imaginary hoppings connect the sites with the same index between the two sublattices and the NHSE is absent. Thus, \mathcal{H} exhibits line-gap spectrum. Under the condition of balanced perturbations, we show exactly that the spectrum of \mathcal{H} are the same as that of H_0 . Notably, the zero modes of H_0 become coalescing states of \mathcal{H} , accompanied by the appearance of EPs. Moreover, other eigenstates of the system can also turn into coalescing states by tuning the real on-site potentials and imaginary hoppings. As a demonstration, we investigate an extended non-Hermitian SSH ladder model. The topological nature of this model can be characterized by the sublattice winding number. We find that the BBC still holds, and with balanced perturbations, the zero-energy edge states become coalescing states with EP in the spectrum. In comparison to the original SSH chain, these edge states are not only robust against local perturbations but also in the time domain, exhibiting self-healing characteristic. Finally, we present numerical results of time evolution to demonstrate that a trivial initial state can always evolve to a dynamically stable topological edge state.

The rest of the paper is organized as follows. In Sec. II, we introduce a class of lattice model and show that the eigenstates can be turned into coalescing states on-demand by modulating the perturbations. In Sec. III,

* zhangkl@fosu.edu.cn

† songtc@nankai.edu.cn

we present an extended SSH model to demonstrate our results, and in Sec. IV, we show that topological edge states are stable in time domain. Finally, conclusions and discussions are given in Sec. V.

II. FORMALISM

We consider a class of tight-binding model consists of a bipartite lattice H_0 , non-Hermitian hoppings and on-site potentials H_p , which can be described by the Hamiltonian as follows

$$\mathcal{H} = H_0 + H_p, \quad (1)$$

with

$$H_0 = \sum_{i \neq j} J_{ij} a_i^\dagger b_j + \text{h.c.}, \quad (2)$$

and

$$H_p = \sum_{j=1}^N \left[i\gamma \left(a_j^\dagger b_j + \text{h.c.} \right) + V \left(a_j^\dagger a_j - b_j^\dagger b_j \right) \right]. \quad (3)$$

This is a bipartite lattice system that can be decomposed into two sublattices with equal site number $N_a = N_b = N$, where a_i^\dagger and b_j^\dagger (a_i and b_j) denote the creation (annihilation) operators on the a and b lattices, and J_{ij} is the hopping strength between the a lattice at i th site and the b lattice at j th site with the constraint

$$J_{ij} = -J_{ji}, \quad (4)$$

which is crucial for the following discussion. $\pm V$ is the on-site potential for the a and b lattices, respectively. The imaginary hopping strength between the a and b with the same site indexes is measured by γ .

In the following, we show that the diagonalization of \mathcal{H} can be resolved from that of H_0 . In fact, H_0 and \mathcal{H} can be written in the following forms

$$H_0 = \Psi^\dagger \begin{pmatrix} \mathbf{0} & T \\ -T & \mathbf{0} \end{pmatrix} \Psi, \quad (5)$$

and

$$\mathcal{H} = \Psi^\dagger \begin{pmatrix} VI_N & T + i\gamma I_N \\ -T + i\gamma I_N & -VI_N \end{pmatrix} \Psi, \quad (6)$$

where Ψ^\dagger is defined as

$$\Psi^\dagger = \left(a_1^\dagger, a_2^\dagger \cdots a_N^\dagger, b_1^\dagger, b_2^\dagger \cdots b_N^\dagger \right), \quad (7)$$

and I_N is the $N \times N$ identity matrix, T is an anti-symmetric $N \times N$ matrix with elements

$$T_{ij} = t_{ij}. \quad (8)$$

It can be checked that the diagonal form of H_0 is

$$H_0 = \sum_{n=1}^N \sum_{\rho=\pm} \rho E_n D_{n,\rho}^\dagger D_{n,\rho}, \quad (9)$$

where $D_{n,\rho}^\dagger$ is defined as

$$D_{n,\pm}^\dagger = \frac{\Psi^\dagger}{\sqrt{2}} \begin{pmatrix} \psi_n \\ \pm i\psi_n \end{pmatrix}, \quad (10)$$

with the $N \times 1$ column vector ψ_n being the eigenstate of the Hermitian matrix iT , that is

$$iT\psi_n = E_n\psi_n. \quad (11)$$

Under the basis of $D_{n,\rho}^\dagger$, the non-Hermitian Hamiltonian \mathcal{H} can be rewritten as

$$\mathcal{H} = \sum_{n=1}^N \left(D_{j,+}^\dagger, D_{j,-}^\dagger \right) \begin{pmatrix} E_n & V + \gamma \\ V - \gamma & -E_n \end{pmatrix} \begin{pmatrix} D_{j,+} \\ D_{j,-} \end{pmatrix}, \quad (12)$$

which can be further diagonalized as

$$\mathcal{H} = \sum_{n=1}^N \sum_{\rho=\pm} \mathcal{E}_{n,\rho} \bar{\mathcal{D}}_{n,\rho} \mathcal{D}_{n,\rho}, \quad (13)$$

where

$$\mathcal{E}_{n,\pm} = \pm \sqrt{E_n^2 + V^2 - \gamma^2}, \quad (14)$$

and

$$\begin{aligned} \bar{\mathcal{D}}_{n,\pm} &= \frac{(E_n + \mathcal{E}_{n,\pm}) D_{n,+}^\dagger + (V - \gamma) D_{n,-}^\dagger}{\sqrt{(E_n + \mathcal{E}_{n,\pm})^2 + V^2 - \gamma^2}}, \\ \mathcal{D}_{n,\pm} &= \frac{(E_n + \mathcal{E}_{n,\pm}) D_{n,+} + (V + \gamma) D_{n,-}}{\sqrt{(E_n + \mathcal{E}_{n,\pm})^2 + V^2 - \gamma^2}}. \end{aligned} \quad (15)$$

Therefore, the eigenstate of \mathcal{H} with eigenenergy $\mathcal{E}_{n,\pm}$ is $\bar{\mathcal{D}}_{n,\pm}|0\rangle$, where $|0\rangle$ is the vacuum state satisfying $a_j|0\rangle = b_j|0\rangle = 0$. Note that $\bar{\mathcal{D}}_{n,\pm} \neq \mathcal{D}_{n,\pm}^\dagger$ for the non-Hermitian case $\gamma \neq 0$. Nevertheless, we note that the system possesses a real spectrum or its eigenvalues always come in complex conjugate pairs, since \mathcal{H} has pseudo-Hermiticity [52], and the spectrum gap is line gap instead of point gap.

These results indicate that we can obtain the solutions of \mathcal{H} via H_0 , and it is worth noting that the conclusion does not depend on the boundary conditions. From the solutions in Eqs. (14) and (15), two conclusions can be drawn: (i) when $V = \pm\gamma$, systems \mathcal{H} and H_0 share the same spectrum, i.e., the non-Hermitian hopping $i\gamma$ counteracts the effects of the on-site potential V from the perspective of energy; (ii) when $E_{n'} = \pm\sqrt{\gamma^2 - V^2}$, we have $\mathcal{E}_{n',\pm} = 0$ and $\bar{\mathcal{D}}_{n',+} = \bar{\mathcal{D}}_{n',-}$, i.e., there are EPs in the spectrum, and two eigenstates coalesce into the same one. In this case, the Hamiltonian in Eq. (12) cannot be

diagonalized, and there will be peculiar dynamic behaviors. Considering the time evolution for an initial state $(\alpha, \beta)_{n'}^T$ in the n' th subspace, the evolved state is

$$\begin{aligned} & \exp \left[-i \begin{pmatrix} E_{n'} & V + \gamma \\ V - \gamma & -E_{n'} \end{pmatrix}_{n'} t \right] \begin{pmatrix} \alpha \\ \beta \end{pmatrix}_{n'} \\ &= \begin{pmatrix} \alpha \\ \beta \end{pmatrix}_{n'} - it \begin{pmatrix} \alpha + \frac{E_{n'}}{\gamma - V} \beta \\ \alpha - \frac{E_{n'}}{\gamma - V} \beta \end{pmatrix} \begin{pmatrix} E_{n'} \\ V - \gamma \end{pmatrix}_{n'}. \end{aligned} \quad (16)$$

We can see that over time, the evolved state tends toward the coalescing mode $\bar{D}_{n',+}|0\rangle$ as long as the initial state has a nonzero overlap with state $(\alpha, \beta)_{n'}^T$ that satisfies $\alpha \neq E_{n'}\beta/(V - \gamma)$. This is called the EP dynamics.

Notably, the EPs are tunable by adjusting the parameters γ and V , and at the same time, the on-site potential V ensures the existence of a full real spectrum. As a result, these EPs can be utilized to generate stable quantum states on demand through the EP dynamics. Particularly, when H_0 is a topological system, this mechanism can be utilized to generate dynamically stable topologically edge states. In the following, we apply this formalism to an extended SSH ladder to demonstrate the above conclusions.

III. EXTENDED SSH MODEL

A. Model and solution

In this section, we consider an extended SSH ladder with non-Hermitian hoppings between the two legs of the ladder, as shown in Fig. 1. The Hamiltonian has the same form as that in Eq. (1), which is

$$\mathcal{H} = H_0 + H_p, \quad (17)$$

where

$$H_0 = \sum_j J_{j,j+1} a_j^\dagger b_{j+1} + \text{h.c.}, \quad (18)$$

and

$$H_p = \sum_j \left[i\gamma \left(a_j^\dagger b_j + \text{h.c.} \right) + V \left(a_j^\dagger a_j - b_j^\dagger b_j \right) \right]. \quad (19)$$

Here the explicit expression of tunneling strength is

$$J_{j,j+1} = -J_{j+1,j} = (-1)^{j+1} \left[1 + (-1)^j \delta \right], \quad (20)$$

and the on-site potential on the a lattice and b lattice is V and $-V$, respectively. Here, $i\gamma$ represents the non-Hermitian hopping.

In the minimal topological model, the SSH chain [53], the topological properties of which arise from the alternating hopping amplitudes, demonstrates a nontrivial topology when the winding number or Zak phase is nonzero [3, 12]. As a result, the boundaries of the system host zero-energy edge states that are protected by

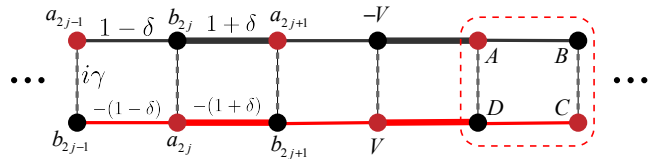


FIG. 1. The Schematic of the extended SSH ladder with imaginary tunneling. The red (black) dots denote lattice sites a (b), with on-site potentials V ($-V$). Each unit cell includes four sites denoted as (A, B, C, D) .

the topology and inversion symmetry of the model. For the extended SSH ladder we are considering, the inversion symmetry is broken by the alternating on-site potential, as in the Rice-Mele model [54]. In the following, we present the solution of the SSH ladder and show that it also supports a topological phase characterized by the sublattice winding number even in the presence of non-Hermitian terms.

Taking periodic boundary conditions for the system with N unit cells, and applying the Fourier transformation

$$\begin{pmatrix} a_{2j-1} \\ b_{2j} \\ a_{2j} \\ b_{2j-1} \end{pmatrix} = \sum_k \frac{e^{ikj}}{\sqrt{N}} \begin{pmatrix} a_{k,1} \\ b_{k,1} \\ a_{k,2} \\ b_{k,2} \end{pmatrix}, \quad (21)$$

where $k = 2\pi n/N$, ($n = 0, 1, \dots, N-1$), then the Hamiltonian can be expressed as

$$\mathcal{H} = \sum_k \Psi^\dagger h_k \Psi, \quad (22)$$

Here, the operator vector is defined as

$$\Psi^\dagger = \left(a_{k,1}^\dagger \quad b_{k,1}^\dagger \quad a_{k,2}^\dagger \quad -b_{k,2}^\dagger \right), \quad (23)$$

and the Bloch Hamiltonian is

$$h_k = \begin{pmatrix} V & \xi_k & 0 & -i\gamma \\ \xi_k^* & -V & i\gamma & 0 \\ 0 & i\gamma & V & \xi_k^* \\ -i\gamma & 0 & \xi_k & -V \end{pmatrix}, \quad (24)$$

where the k -dependent parameter is given by

$$\xi_k = 1 - \delta + (1 + \delta) e^{-ik}. \quad (25)$$

The Hamiltonian respects the following symmetry

$$SK h_k (SK)^{-1} = h_k, \quad (26)$$

where

$$S = \begin{pmatrix} 0 & 0 & 1 & 0 \\ 0 & 0 & 0 & 1 \\ 1 & 0 & 0 & 0 \\ 0 & 1 & 0 & 0 \end{pmatrix}, \quad (27)$$

and K is the complex conjugate operator defined as $KiK = -i$. This means that for an eigenstate $|\psi\rangle$ of h_k with eigenenergy ε_k , the state $SK|\psi\rangle$ is also the eigenstate of h_k with the same eigenvalue, i.e., the spectrum is at least two-fold degenerate. Actually, the eigenstates and eigenenergies of h_k can be given as

$$|\psi_1\rangle = \Omega_1 \begin{pmatrix} \xi_k \\ \varepsilon_k^- - V \\ i\gamma \\ 0 \end{pmatrix}, |\psi_2\rangle = \Omega_2 \begin{pmatrix} \varepsilon_k^- + V \\ \xi_k^* \\ 0 \\ -i\gamma \end{pmatrix}, \quad (28)$$

with eigenenergy

$$\varepsilon_k^- = -\sqrt{\xi_k \xi_k^* + V^2 - \gamma^2}, \quad (29)$$

and

$$|\psi_3\rangle = \Omega_3 \begin{pmatrix} \xi_k \\ \varepsilon_k^+ - V \\ i\gamma \\ 0 \end{pmatrix}, |\psi_4\rangle = \Omega_4 \begin{pmatrix} \varepsilon_k^+ + V \\ \xi_k^* \\ 0 \\ -i\gamma \end{pmatrix}, \quad (30)$$

with eigenenergy

$$\varepsilon_k^+ = \sqrt{\xi_k \xi_k^* + V^2 - \gamma^2}. \quad (31)$$

Here Ω_α , $\alpha = 1, 2, 3, 4$, are the corresponding normalization constants. Obviously, as discussed in the previous section, when $\xi_k \xi_k^* = \gamma^2 - V^2$, there are EPs in the spectrum, and $\varepsilon_k^+ = \varepsilon_k^- = 0$. In this case, two pairs of degenerate eigenstates coalesce into two eigenstates

$$|\psi_1\rangle = |\psi_3\rangle, |\psi_2\rangle = |\psi_4\rangle. \quad (32)$$

B. Sublattice winding number

To characterize the topology of the extended SSH ladder without inversion symmetry and chiral symmetry, we employ the sublattice winding number [15–17], which is defined as

$$w_\epsilon^\rho = \frac{1}{2\pi i} \oint_{\text{BZ}} dk \text{Tr} \left[P_\rho (h_k - \epsilon)^{-1} \partial_k (h_k - \epsilon) P_\rho \right], \quad (33)$$

where ρ represents the sublattice index. For the SSH ladder shown in Fig. 1, there are four sublattices in every unit cell, that is $\rho = A, B, C, D$, and $P_\rho = |\rho\rangle\langle\rho|$ is the projection operator with

$$|\rho\rangle = (\delta_{\rho,A}, \delta_{\rho,B}, \delta_{\rho,C}, \delta_{\rho,D})^T. \quad (34)$$

Taking the reference energy as $\epsilon = \pm\sqrt{V^2 - \gamma^2}$, direct derivations show that (see Appendix A)

$$w_\epsilon^A = \int_0^{2\pi} \frac{dk}{2\pi i} \partial_k \log(\xi_k^*) = \begin{cases} 0, & \delta < 0 \\ 1, & \delta > 0 \end{cases}, \\ w_\epsilon^B = \int_0^{2\pi} \frac{dk}{2\pi i} \partial_k \log(\xi_k) = \begin{cases} 0, & \delta < 0 \\ -1, & \delta > 0 \end{cases}, \quad (35)$$

and

$$w_\epsilon^D = w_\epsilon^A, w_\epsilon^C = w_\epsilon^B. \quad (36)$$

Furthermore, one can define a topological invariant

$$w^A = \sum_\epsilon w_\epsilon^A, \quad (37)$$

the nontrivial value of which equals the number of edge states distributed at each end of the system. For the SSH ladder, the reference energy is two-fold degenerate, therefore

$$w^A = 2w_\epsilon^A. \quad (38)$$

This indicates that there are 2 edge states localized at each end of the system. The topological edge states can be exactly solved and are dynamically stable, as shown in the next section.

IV. DYNAMICALLY STABLE TOPOLOGICAL EDGE STATES

Now we investigate the edge states and their dynamic behavior for the SSH ladder. When taking the open boundary conditions, according to the discussions in Sec. II, the eigenenergies of \mathcal{H} are

$$\mathcal{E}_\pm = \pm\sqrt{E_0^2 + V^2 - \gamma^2}, \quad (39)$$

where E_0 is the eigenenergy of H_0 , and for the edge states of the SSH chain, we have $E_0 = 0$. Thus, for the SSH ladder \mathcal{H} , the energies of the edge states are $\mathcal{E}_\pm = \pm\sqrt{V^2 - \gamma^2}$.

We set the ansatz of the edge state as the following form

$$|\psi\rangle = \sum_{l=1}^{2N} \left(\alpha_l a_l^\dagger + \beta_l b_l^\dagger \right) |0\rangle, \quad (40)$$

and substituting it and \mathcal{H} into the Schrödinger equation

$$\mathcal{H}|\psi\rangle = \pm\sqrt{V^2 - \gamma^2}|\psi\rangle. \quad (41)$$

Under the condition of $N \rightarrow \infty$ and $0 < \delta < 1$, by solving the Schrödinger equation in Eq. (B2), we obtain four edge states (see Appendix B for the details)

$$|\psi_L^\pm\rangle = \Omega_L^\pm \sum_{j=1}^N (-1)^{j-1} e^{-(j-1)\zeta} \left(\kappa_\pm a_{2j-1}^\dagger + b_{2j-1}^\dagger \right) |0\rangle,$$

$$|\psi_R^\pm\rangle = \Omega_R^\pm \sum_{j=1}^N (-1)^{N-j} e^{-(N-j)\zeta} \left(\kappa_\pm a_{2j}^\dagger + b_{2j}^\dagger \right) |0\rangle, \quad (42)$$

with $\Omega_{L/R}^\pm$ being the normalization constant. Like the SSH chain, the amplitudes in Eq. (42) are distributed

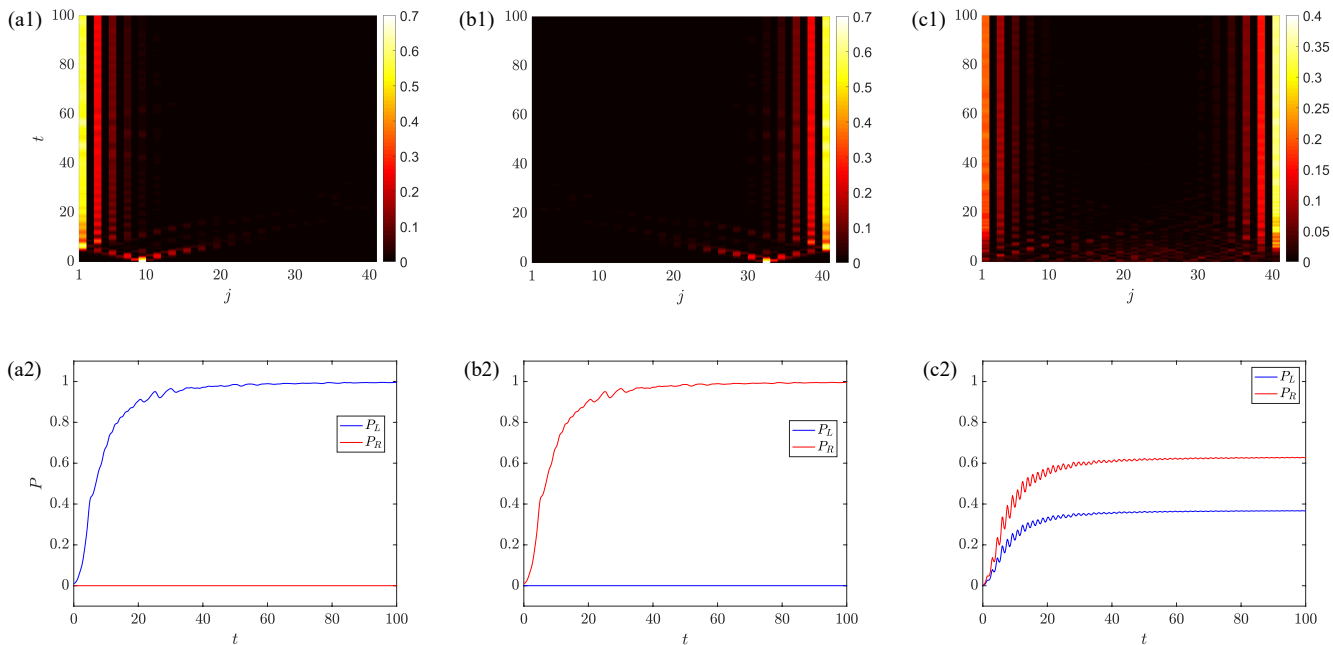


FIG. 2. The spatial distribution of the modulus of the amplitudes of the evolved state (top panels) and the plots of the overlap between the evolved state and two edge states as a function of time (bottom panels). For (a1) and (b1), the initial states are two point excitations localized at the site near the left end (the 9th site) and the right end (the 32nd site) of the system, respectively. For (c1), the initial state is a state with a random distribution. (a2), (b2) and (c2) give the corresponding overlap between the evolved state and the left edge state (P_L) and the right edge state (P_R) as a function of time. Other parameters are taken as $N = 20$, $V = \gamma = 1$, and $\delta = 0.2$.

at the lattice sites with odd (even) index for edge states localized at the left (right) of the ladder. While the relative amplitudes for lattices a and b at the same index are modulated by κ_{\pm} , which is defined as

$$\kappa_{\pm} = \frac{-i\gamma}{V \mp \sqrt{V^2 - \gamma^2}}. \quad (43)$$

The amplitudes of edge states exhibit exponential decay, and the localization length is $\zeta = \ln[(\delta + 1)/(1 - \delta)] > 0$, ($0 < \delta < 1$). The above results are consistent with the results of the sublattice winding number obtained in the previous section, establishing the BBC. Obviously, when $|V| = |\lambda|$, the spectrum is fully real, and there are EPs for the zero energy edge states. In this case

$$\kappa_+ = \kappa_-, \quad (44)$$

thus, two pairs of edge states coalesce to two edge states

$$|\psi_L^+\rangle = |\psi_L^-\rangle, |\psi_R^+\rangle = |\psi_R^-\rangle. \quad (45)$$

The above two coalescing edge states are dynamically stable due to the EP dynamics introduced in Sec. II. This can be verified by the numerical computation of time evolution for the time-dependent Schrödinger equation. Considering an arbitrary initial state in the following form

$$|\psi(0)\rangle = \phi^\dagger \psi|0\rangle, \quad (46)$$

where

$$\phi^\dagger = \left(a_1^\dagger, b_2^\dagger \cdots b_{2N}^\dagger, b_1^\dagger, a_2^\dagger \cdots a_{2N}^\dagger \right), \quad (47)$$

and ψ is a $4N \times 1$ column vector. In the topological phase with EP, one can expect that the initial state will converge to a stable edge state composed of two coalescing states after a sufficiently long time. To verify this prediction, numerical results for different initial states are presented in Fig. 2. The normalized evolved state is $|\psi(t)\rangle = e^{-i\mathcal{H}t} |\psi(0)\rangle / |e^{-i\mathcal{H}t} |\psi(0)\rangle|$, and the numerical computations are performed by using a uniform mesh for time discretization. The top panels of Fig. 2 show the time evolution of the modulus of the normalized amplitudes $|\langle j | \psi(t) \rangle|^2$, where $|j\rangle = (a_j^\dagger + b_j^\dagger)|0\rangle$. The bottom panels show the results of modulus of overlaps between the evolved state and the normalized edge states in Eq. (42), that is $P_{L/R} = |\langle \psi_{L/R}^\pm | \psi(t) \rangle|^2$. Parameters of the system are taken as $N = 20$, $V = \gamma = 1$, and $\delta = 0.2$.

Figs. 2(a) and (b) demonstrate that if the initial point excitation localized at the left (right) of the system, then the stable final state would converge to the left (right) edge state. In addition, Fig. 2(c) show that an initial state with random amplitude distribution would evolve to an edge state distributed on the two ends of the system.

In order to investigate the robustness of the edge state in time domain, we apply a global quench to parameter

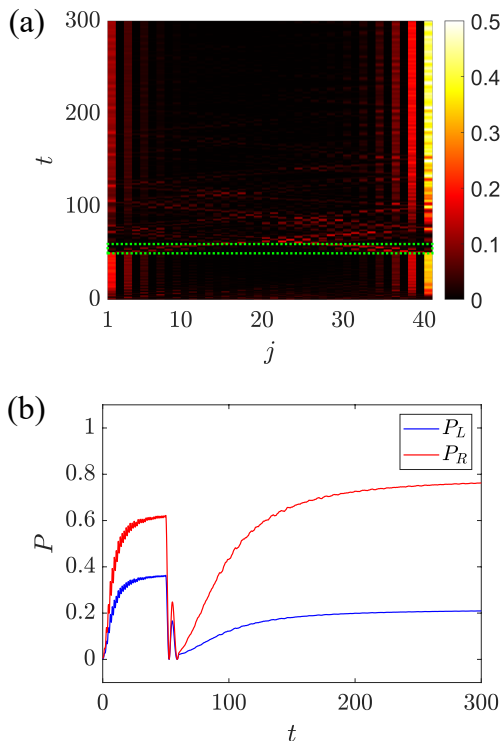


FIG. 3. (a) The spatial distribution of the modulus of the amplitudes of the evolved state. The initial state is a state with a random distribution, the same as that in Fig. 2 (c1), and the parameter of the initial Hamiltonian is $\delta = 0.2$. While there is a perturbation in the temporal interval $t \in [50, 60]$ marked by the green dashed rectangle, in which the system is quenched to the parameter $\delta = -0.2$. (b) The plot of the overlap between the evolved state and two edge states as a function of time. Other parameters are taken as $N = 20$ and $V = \gamma = 1$.

δ in a temporal interval. The initial state and Hamiltonian are taken to be the same as that in Fig. 2 (c1). While at $t = 50$, δ is switched from 0.2 to -0.2 , which corresponds to the topologically trivial phase, and at $t = 60$, δ is switched back to 0.2. The numerical results of this quenching process are shown in Fig. 3. We can see that the formed edge state is disrupted in the temporal interval $t \in [50, 60]$, and gradually recovers after $t = 60$. These numerical results indicate that the zero-energy edge states in the SSH ladder are robust in the time domain.

V. CONCLUSION

In summary, we have shown that in a class of non-Hermitian bipartite lattices, the imaginary hopping and staggered on-site potential can be utilized to generate tunable EP with two eigenstates coalescing into the same one. We apply this mechanism to generate dynamically

stable topological edge states in an extended SSH ladder with balanced imaginary hopping and on-site potential. In this model, the zero-energy edge states are characterized by the sublattice winding number, and are not only robust against local perturbations but also in the time domain. Numerical results demonstrate that a trivial initial state can always evolve into a stable topological edge state. Our results provide insights for the application of time-domain stable topological quantum devices.

ACKNOWLEDGMENTS

This work was supported by the National Natural Science Foundation of China (under Grant No. 12374461).

APPENDIX A: CALCULATION OF THE SUBLATTICE WINDING NUMBER

In this appendix, we present the detailed calculation about the sublattice winding number. According to Eq. (24) we have

$$\frac{1}{h_k - \epsilon} = \begin{pmatrix} \frac{V+\epsilon}{\xi\xi^*} & \frac{1}{\xi^*} & 0 & \frac{-i\gamma}{\xi\xi^*} \\ \frac{1}{\xi} & \frac{V-\epsilon}{-\xi\xi^*} & \frac{i\gamma}{\xi\xi^*} & 0 \\ 0 & \frac{i\gamma}{\xi\xi^*} & \frac{V+\epsilon}{\xi\xi^*} & \frac{1}{\xi} \\ \frac{-i\gamma}{\xi\xi^*} & 0 & \frac{1}{\xi^*} & \frac{V-\epsilon}{-\xi\xi^*} \end{pmatrix}, \quad (\text{A1})$$

where $\epsilon = \pm\sqrt{V^2 - \gamma^2}$ and

$$\partial_k (h_k - \epsilon) = \begin{pmatrix} 0 & \frac{\partial\xi}{\partial k} & 0 & 0 \\ \frac{\partial\xi^*}{\partial k} & 0 & 0 & 0 \\ 0 & 0 & 0 & \frac{\partial\xi^*}{\partial k} \\ 0 & 0 & \frac{\partial\xi}{\partial k} & 0 \end{pmatrix}, \quad (\text{A2})$$

then we have

$$\text{diag} \left[(h_k - \epsilon)^{-1} \partial_k (h_k - \epsilon) \right] = \begin{pmatrix} \Gamma & 0 \\ 0 & \Gamma^\dagger \end{pmatrix}, \quad (\text{A3})$$

where

$$\Gamma = \begin{pmatrix} \frac{\partial \log(\xi^*)}{\partial k} & 0 \\ 0 & \frac{\partial \log(\xi)}{\partial k} \end{pmatrix}. \quad (\text{A4})$$

According to the definition of the sublattice winding number in Eq. (33), we have

$$w_\epsilon^A = \int_0^{2\pi} \frac{dk}{2\pi i} \partial_k \log(\xi^*),$$

$$w_\epsilon^B = \int_0^{2\pi} \frac{dk}{2\pi i} \partial_k \log(\xi). \quad (\text{A5})$$

Similarly, we get

$$w_\epsilon^D = w_\epsilon^A,$$

$$w_\epsilon^C = w_\epsilon^B. \quad (\text{A6})$$

Further calculation shows that

$$\begin{aligned} w_\epsilon^A &= \begin{cases} 0, \delta < 0 \\ 1, \delta > 0 \end{cases}, \\ w_\epsilon^B &= \begin{cases} 0, \delta < 0 \\ -1, \delta > 0 \end{cases}, \end{aligned} \quad (\text{A7})$$

and

$$w^A = 2w_\epsilon^A = \begin{cases} 0, \delta < 0 \\ 2, \delta > 0 \end{cases}. \quad (\text{A8})$$

APPENDIX B: SOLUTION OF THE EDGE STATES

Here we present the detailed derivation of the edge states of the SSH ladder \mathcal{H} . The ansatz of the edge state can be taken as

$$|\psi\rangle = \sum_{l=1}^{2N} \left(\alpha_l a_l^\dagger + \beta_l b_l^\dagger \right) |0\rangle. \quad (\text{B1})$$

Substituting it and \mathcal{H} into

$$\mathcal{H}|\psi\rangle = \pm\sqrt{V^2 - \gamma^2}|\psi\rangle, \quad (\text{B2})$$

we obtain

$$\begin{aligned} (1 - \delta)\beta_{2j+2} + (1 + \delta)\beta_{2j} + \chi_{j+1}^\pm &= 0, \\ (1 - \delta)\alpha_{2j+2} + (1 + \delta)\alpha_{2j} + \kappa_\pm\chi_{j+1}^\pm &= 0, \\ (1 + \delta)\alpha_{2j+1} + (1 - \delta)\alpha_{2j-1} + \kappa_\pm\eta_j^\pm &= 0, \\ (1 + \delta)\beta_{2j+1} + (1 - \delta)\beta_{2j-1} + \eta_j^\pm &= 0, \end{aligned} \quad (\text{B3})$$

for $j \in [1, N - 1]$, and

$$\begin{aligned} (1 - \delta)\beta_2 + \chi_1^\pm &= 0, \\ (1 - \delta)\alpha_2 + \kappa_\pm\chi_1^\pm &= 0, \\ (1 - \delta)\alpha_{2N-1} + \kappa_\pm\eta_N^\pm &= 0, \\ (1 - \delta)\beta_{2N-1} + \eta_N^\pm &= 0, \end{aligned} \quad (\text{B4})$$

for the boundary terms. Here

$$\begin{aligned} \chi_j^\pm &= (V - \mathcal{E}_\pm)\alpha_{2j-1} + i\gamma\beta_{2j-1}, \\ \eta_j^\pm &= (\mathcal{E}_\pm - V)\alpha_{2j} - i\gamma\beta_{2j}, \end{aligned} \quad (\text{B5})$$

for $j \in [1, N]$, and κ_\pm are defined as

$$\kappa_\pm = \frac{-i\gamma}{V \mp \sqrt{V^2 - \gamma^2}}. \quad (\text{B6})$$

Combining Eq. (B3) and Eq. (B4), we can get the following equations

$$\begin{aligned} (1 - \delta)\beta_{2j+2} + (1 + \delta)\beta_{2j} &= 0, \\ (1 + \delta)\alpha_{2j+1} + (1 - \delta)\alpha_{2j-1} &= 0, \end{aligned} \quad (\text{B7})$$

for $j \in [1, N - 1]$, and

$$\beta_2 = 0, \alpha_{2N-1} = 0. \quad (\text{B8})$$

Here

$$\alpha_l = \kappa_\pm\beta_l, \quad (\text{B9})$$

with $l \in [1, 2N]$.

Thus, under the large N limit and with condition $0 < \delta < 1$, there are four edge eigenstates localized at the two ends of the system, which have the form

$$\begin{aligned} |\psi_L^\pm\rangle &= \sum_{j=1}^N \left(\alpha_{2j-1} a_{2j-1}^\dagger + \beta_{2j-1} b_{2j-1}^\dagger \right) |0\rangle, \\ |\psi_R^\pm\rangle &= \sum_{j=1}^N \left(\alpha_{2j} a_{2j}^\dagger + \beta_{2j} b_{2j}^\dagger \right) |0\rangle, \end{aligned} \quad (\text{B10})$$

where the parameters satisfy

$$\begin{aligned} \alpha_{2j-1}(\beta_{2j-1}) &= (-1)^{j-1} e^{-(j-1)\zeta} \alpha_1(\beta_1), j \in [2, N], \\ \alpha_{2j}(\beta_{2j}) &= (-1)^{N-j} e^{-(N-j)\zeta} \alpha_{2N}(\beta_{2N}), j \in [1, N - 1], \\ \alpha_l &= \kappa_\pm\beta_l, l \in [1, 2N], \end{aligned} \quad (\text{B11})$$

and the localization length is $\zeta = \ln[(\delta + 1)/(1 - \delta)] > 0$ ($0 < \delta < 1$).

-
- [1] K. v. Klitzing, G. Dorda, and M. Pepper, New method for high-accuracy determination of the fine-structure constant based on quantized hall resistance, *Phys. Rev. Lett.* **45**, 494 (1980).
- [2] D. J. Thouless, M. Kohmoto, M. P. Nightingale, and M. den Nijs, Quantized hall conductance in a two-dimensional periodic potential, *Phys. Rev. Lett.* **49**, 405 (1982).
- [3] J. Zak, Berry's phase for energy bands in solids, *Phys. Rev. Lett.* **62**, 2747 (1989).
- [4] A. Y. Kitaev, Unpaired majorana fermions in quantum wires, *Phys. Usp.* **44**, 131 (2001).
- [5] L. Fu and C. L. Kane, Topological insulators with inversion symmetry, *Phys. Rev. B* **76**, 045302 (2007).
- [6] C. Nayak, S. H. Simon, A. Stern, M. Freedman, and S. Das Sarma, Non-abelian anyons and topological quantum computation, *Rev. Mod. Phys.* **80**, 1083 (2008).
- [7] X.-L. Qi and S.-C. Zhang, Topological insulators and superconductors, *Rev. Mod. Phys.* **83**, 1057 (2011).
- [8] S. Matsuura, P.-Y. Chang, A. P. Schnyder, and S. Ryu, Protected boundary states in gapless topological phases, *New J. Phys.* **15**, 065001 (2013).
- [9] C.-K. Chiu and A. P. Schnyder, Classification of reflection-symmetry-protected topological semimetals

- and nodal superconductors, *Phys. Rev. B* **90**, 205136 (2014).
- [10] S. D. Sarma, M. Freedman, and C. Nayak, Majorana zero modes and topological quantum computation, *npj Quantum Information* **1**, 1 (2015).
- [11] C.-K. Chiu, J. C. Y. Teo, A. P. Schnyder, and S. Ryu, Classification of topological quantum matter with symmetries, *Rev. Mod. Phys.* **88**, 035005 (2016).
- [12] J. K. Asbóth, L. Oroszlány, and A. Pályi, *A short course on topological insulators* (Springer, 2016).
- [13] S. Kobayashi, S. Sumita, Y. Yanase, and M. Sato, Symmetry-protected line nodes and majorana flat bands in nodal crystalline superconductors, *Phys. Rev. B* **97**, 180504 (2018).
- [14] L. Xie, L. Jin, and Z. Song, Antihelical edge states in two-dimensional photonic topological metals, *Sci. Bull.* **68**, 255 (2023).
- [15] J.-W. Rhim, J. Behrends, and J. H. Bardarson, Bulk-boundary correspondence from the intercellular zak phase, *Phys. Rev. B* **95**, 035421 (2017).
- [16] M. Guzmán, D. Bartolo, and D. Carpentier, Geometry and topology tango in ordered and amorphous chiral matter, *SciPost Phys.* **12**, 038 (2022).
- [17] S. Verma and T. K. Ghosh, Bulk-boundary correspondence in extended trimer su-schrieffer-heeger model, *Phys. Rev. B* **110**, 125424 (2024).
- [18] D. V. Else, P. Fendley, J. Kemp, and C. Nayak, Prethermal strong zero modes and topological qubits, *Phys. Rev. X* **7**, 041062 (2017).
- [19] M. C. Rechtsman, J. M. Zeuner, Y. Plotnik, Y. Lumer, D. Podolsky, F. Dreisow, S. Nolte, M. Segev, and A. Szameit, Photonic floquet topological insulators, *Nature* **496**, 196 (2013).
- [20] M. Lohse, C. Schweizer, H. M. Price, O. Zilberberg, and I. Bloch, Exploring 4d quantum hall physics with a 2d topological charge pump, *Nature* **553**, 55 (2018).
- [21] W. Sun, C.-R. Yi, B.-Z. Wang, W.-W. Zhang, B. C. Sanders, X.-T. Xu, Z.-Y. Wang, J. Schmiedmayer, Y. Deng, X.-J. Liu, S. Chen, and J.-W. Pan, Uncover topology by quantum quench dynamics, *Phys. Rev. Lett.* **121**, 250403 (2018).
- [22] D.-W. Zhang, Y.-Q. Zhu, Y. Zhao, H. Yan, and S.-L. Zhu, Topological quantum matter with cold atoms, *Adv. Phys.* **67**, 253 (2018).
- [23] J. Li, A. K. Harter, J. Liu, L. de Melo, Y. N. Joglekar, and L. Luo, Observation of parity-time symmetry breaking transitions in a dissipative Floquet system of ultracold atoms, *Nat. Commun.* **10**, 855 (2019).
- [24] S. Barbarino, J. Yu, P. Zoller, and J. C. Budich, Preparing atomic topological quantum matter by adiabatic nonunitary dynamics, *Phys. Rev. Lett.* **124**, 010401 (2020).
- [25] M. S. Rudner and N. H. Lindner, Band structure engineering and non-equilibrium dynamics in floquet topological insulators, *Nat. Rev. Phys.* **2**, 229 (2020).
- [26] L. Zhang, L. Zhang, and X.-J. Liu, Unified theory to characterize floquet topological phases by quench dynamics, *Phys. Rev. Lett.* **125**, 183001 (2020).
- [27] R. Citro and M. Aidelsburger, Thouless pumping and topology, *Nat. Rev. Phys.* **5**, 87 (2023).
- [28] Q. Bin, L.-L. Wan, F. Nori, Y. Wu, and X.-Y. Lü, Out-of-time-order correlation as a witness for topological phase transitions, *Phys. Rev. B* **107**, L020202 (2023).
- [29] T. L. M. Lane, M. Horváth, and K. Patrick, Extended edge modes and disorder preservation of a symmetry-protected topological phase out of equilibrium, *Phys. Rev. B* **110**, 165139 (2024).
- [30] L. Jin, Topological phases and edge states in a non-hermitian trimerized optical lattice, *Phys. Rev. A* **96**, 032103 (2017).
- [31] K. Takata and M. Notomi, Photonic topological insulating phase induced solely by gain and loss, *Phys. Rev. Lett.* **121**, 213902 (2018).
- [32] G. Harari, M. A. Bandres, Y. Lumer, M. C. Rechtsman, Y. D. Chong, M. Khajavikhan, D. N. Christodoulides, and M. Segev, Topological insulator laser: theory, *Science* **359**, 10.1126/science.aar4003 (2018).
- [33] M. A. Bandres, S. Wittek, G. Harari, M. Parto, J. Ren, M. Segev, D. N. Christodoulides, and M. Khajavikhan, Topological insulator laser: Experiments, *Science* **359**, 10.1126/science.aar4005 (2018).
- [34] S. Yao, F. Song, and Z. Wang, Non-hermitian chern bands, *Phys. Rev. Lett.* **121**, 136802 (2018).
- [35] S. Yao and Z. Wang, Edge states and topological invariants of non-hermitian systems, *Phys. Rev. Lett.* **121**, 086803 (2018).
- [36] L. Jin and Z. Song, Bulk-boundary correspondence in a non-hermitian system in one dimension with chiral inversion symmetry, *Phys. Rev. B* **99**, 081103 (2019).
- [37] C. H. Lee and R. Thomale, Anatomy of skin modes and topology in non-hermitian systems, *Phys. Rev. B* **99**, 201103 (2019).
- [38] X.-W. Luo and C. Zhang, Higher-order topological corner states induced by gain and loss, *Phys. Rev. Lett.* **123**, 073601 (2019).
- [39] X. Zhang and J. Gong, Non-hermitian floquet topological phases: Exceptional points, coalescent edge modes, and the skin effect, *Phys. Rev. B* **101**, 045415 (2020).
- [40] L. Zhou and Q. Du, Non-hermitian topological phases and dynamical quantum phase transitions: A generic connection, *New J. Phys.* **23**, 063041 (2021).
- [41] H. C. Wu, L. Jin, and Z. Song, Topology of an anti-parity-time symmetric non-hermitian su-schrieffer-heeger model, *Phys. Rev. B* **103**, 235110 (2021).
- [42] F. Roccati, M. Bello, Z. Gong, M. Ueda, F. Ciccarello, A. Chenu, and A. Carollo, Hermitian and non-hermitian topology from photon-mediated interactions, *Nat. Commun.* **15**, 2400 (2024).
- [43] L. Huang, S. Huang, C. Shen, S. Yves, A. S. Pilipchuk, X. Ni, S. Kim, Y. K. Chiang, D. A. Powell, J. Zhu, *et al.*, Acoustic resonances in non-hermitian open systems, *Nat. Rev. Phys.* **6**, 11 (2024).
- [44] K. L. Zhang, P. Wang, and Z. Song, Exceptional-point-induced lasing dynamics in a non-hermitian su-schrieffer-heeger model, *Phys. Rev. A* **99**, 042111 (2019).
- [45] K. L. Zhang, L. Jin, and Z. Song, Helical resonant transport and purified amplification at an exceptional point, *Phys. Rev. B* **100**, 144301 (2019).
- [46] C. Wang, W. R. Sweeney, A. D. Stone, and L. Yang, Coherent perfect absorption at an exceptional point, *Science* **373**, 1261 (2021).
- [47] P. Wang, K. L. Zhang, and Z. Song, Transition from degeneracy to coalescence: Theorem and applications, *Phys. Rev. B* **104**, 245406 (2021).
- [48] Y. Shi, K. Zhang, and Z. Song, Exceptional spectrum and dynamic magnetization, *J. Phys.:Condens. Matter* **34**, 485401 (2022).
- [49] S. Longhi, Self-healing of non-hermitian topological skin

- modes, *Phys. Rev. Lett.* **128**, 157601 (2022).
- [50] W.-T. Xue, F. Song, Y.-M. Hu, and Z. Wang, Non-bloch edge dynamics of non-hermitian lattices, arXiv preprint arXiv:2503.13671 (2025).
- [51] Y. Miao, Y. Zhao, Y. Wang, J. Qiao, X. Zhao, and X. Yi, Non-abelian gauge enhances self-healing for non-hermitian su–schrieffer–heeger chain, arXiv preprint arXiv:2503.23978 (2025).
- [52] A. Mostafazadeh, Pseudo-hermiticity versus pt-symmetry iii: Equivalence of pseudo-hermiticity and the presence of antilinear symmetries, *J. Math. Phys.* **43**, 3944 (2002).
- [53] W. P. Su, J. R. Schrieffer, and A. J. Heeger, Solitons in polyacetylene, *Phys. Rev. Lett.* **42**, 1698 (1979).
- [54] M. J. Rice and E. J. Mele, Elementary excitations of a linearly conjugated diatomic polymer, *Phys. Rev. Lett.* **49**, 1455 (1982).